 doi:10.20944/preprints202205.0122.v1

Article

Series with Binomial-Like Coefficients for the Investigation of Fractal Structures Associated with the Riemann Zeta Function

Igoris Belovas [1,*], Martynas Sabaliauskas [2] and Lukas Kuzma [3]

[1] Institute of Data Science and Digital Technologies, Faculty of Mathematics and Informatics, Vilnius University, LT-04812 Vilnius, Lithuania; igoris.belovas@mif.vu.lt (I.B.)
[2] Institute of Data Science and Digital Technologies, Faculty of Mathematics and Informatics, Vilnius University, LT-04812 Vilnius, Lithuania; martynas.sabaliauskas@mif.vu.lt (M.S.)
[3] Institute of Data Science and Digital Technologies, Faculty of Mathematics and Informatics, Vilnius University, LT-04812 Vilnius, Lithuania; lukas.kuzma@mif.vu.lt (L.K.)
* Correspondence: igoris.belovas@mif.vu.lt

Abstract: The paper continues the study of efficient algorithms for the computation of zeta functions over the complex plane. We aim to apply the modifications of algorithms to the investigation of underlying fractal structures associated with the Riemann zeta function. We discuss the computational complexity and numerical aspects of the implemented algorithms based on series with binomial-like coefficients.

Keywords: Riemann zeta function; fractal structures; numerical algorithms

1. Introduction

In this paper, we continue the study of efficient algorithms for the computation of the Riemann zeta function over the complex plane, introduced by Borwein [7] and extended by Belovas [1], Belovas and Sabaliauskas [4], Belovas, Sakalauskas and Starikovičius [5]. Šleževičienė [14], Vepštas [16] and Coffey [8] applied this methodology for the computation of Dirichlet L-functions, Hurwitz zeta function and polylogarithm. Belovas [1], Belovas and Sabaliauskas [4] obtained limit theorems, which allowed the introduction of asymptotic approximations for the coefficients of the series of the algorithms. A preliminary presentation of computational aspects of the approach has been presented in [5]. Theoretical aspects of the approach (as well as more subtle proofs of the limit theorems) have been discussed in [2] and [3].

Fractal geography of the Riemann zeta function (and other zeta functions) was addressed by King [11]. Woon [17] and Tingen [15] computed Julia and Mandelbrot sets of the Riemann zeta function and Hurwitz zeta function, respectively, and studied the properties of these fractals. Recently Blankers et al. [6] investigated the analogs of Julia and Mandelbrot sets for dynamical systems over the hyperbolic numbers. In the present study, we enhance algorithms for the calculation of the Riemann zeta function, proposed in [4] and [5]. We specify the convergence rate to the limiting distribution for the coefficients of the series, identify the error term and discuss computational complexity. The algorithms are compared against the recently proposed *Zetafast* algorithm [9] and are applied for the investigation of underlying fractal structures associated with the Riemann zeta function.

The paper is organized as follows. The first part is the introduction. In Section 2, we describe algorithms and present theoretical results. Section 3 is devoted to the visual investigation of the underlying fractal background of the Riemann zeta function. Pseudocodes of the algorithms for the computation and the visualization are given in Section 4. Section 5 and Section 6 are devoted to presenting the results and conclusions, respectively.

Preprints (www.preprints.org) | NOT PEER-REVIEWED | Posted: 10 May 2022 doi:10.20944/preprints202205.0122.v1

Throughout this paper, we denote by $\Phi(x)$ the cumulative distribution function of the standard normal distribution, and by $\overline{\Phi}(x)$ we denote the corresponding tail distribution $\overline{\Phi}(x) = 1 - \Phi(x)$. $\Gamma(s)$, $B(x,y)$ and $W(x)$ denote the gamma function, the beta function and the Lambert W function respectively. $I_x(a,b)$ stands for the regularized incomplete beta function,

$$I_x(a,b) = \frac{1}{B(a,b)} \int_0^x t^{a-1}(1-t)^{b-1}dt.$$

C_n^k are the binomial coefficients. $\lfloor x \rfloor$ and $\lceil x \rceil$ stand for the floor function and the ceiling functions respectively. $A \times B$ stands for the Cartesian product of two sets A and B. All limits in the paper, unless specified, are taken as $n \to \infty$.

2. *MB*- and *BLC*-algorithms for the computation of the Riemann zeta function

MB-algorithm

In [5] Belovas et al. proposed a modification of Borwein's efficient algorithm (*MB*-algorithm) for the Riemann zeta function [7]. The algorithm applies to complex numbers $s = \sigma + it$ with $\sigma \geqslant 1/2$ and arbitrary t. Let us denote, along with Proposition 1 from [5],

$$l_{max} = \arg\max_{0 \leqslant k \leqslant n} \frac{(n+k-1)!4^k}{(n-k)!(2k)!} \quad \text{and} \quad c_{n,k}^{(1)} = 1 - \frac{H_k}{H_n}, \quad n \in \mathbb{N}, \ 0 \leqslant k \leqslant n, \tag{1}$$

here

$$\begin{aligned} H_l &= H_{l-1} + \exp(T_l - T_{l_{max}} + (l - l_{max})\log 4), & H_0 &= \exp(T_0 - T_{l_{max}} - l_{max}\log 4), \\ T_l &= T_{l-1} + \log\frac{(n-l+1)(n+l-1)}{(2l-1)(2l)}, & T_0 &= -\log n, \quad 1 \leqslant l \leqslant n. \end{aligned} \tag{2}$$

Under these notations (case $j = 1$ in $c_{n,k}^{(j)}$ corresponds *MB*-series) the Riemann zeta function is

$$\zeta(s) = \frac{1}{1-2^{1-s}} \sum_{k=0}^{n-1} \frac{(-1)^k c_{n,k}^{(j)}}{(k+1)^s} + \gamma_n^{(j)}(s). \tag{3}$$

The algorithm is nearly optimal in the sense that there is no sequence of n-term exponential polynomials that converge to the Riemann zeta function much faster than of the algorithm (see Theorem 3.1 in [7]).

BLC-algorithm

This algorithm, introduced in [4], also uses series (3) (case $j = 2$), but with different binomial-like coefficients,

$$c_{n,k}^{(2)} = I_{1/2}(k+1, n-k+1). \tag{4}$$

The error terms $\gamma_n^{(j)}(s)$ of these methods are discussed in the following subsection.

Error terms and computational complexity

First we formulate an auxiliary lemma, aiming to investigate the behaviour of the series in the neighbourhoods of critical points s_k (note that $1 - 2^{1-s} = 0$ if and only if $t = 2\pi k/\log 2$, $k \in \mathbb{Z}$ and $\sigma = 1$).

Lemma 1. *Let* $r_0 = 3$ *and*

$$s_k = 1 + 2i\pi k/\log 2, \qquad k \in \mathbb{N}_0. \tag{5}$$

Preprints (www.preprints.org) | NOT PEER-REVIEWED | Posted: 10 May 2022 doi:10.20944/preprints202205.0122.v1

Let ω_k be the circle

$$\omega_k = \{s : \ |s - s_k| = \rho > 0\}.$$

Then, for $f(s) = 1/(1 - 2^{1-s})$ and $\rho \leqslant r_0/\log 2$,

$$\max_{s\in\omega_k} |f(s)| \leqslant \frac{1}{1 - 2^{-\rho}}. \tag{6}$$

Proof of Lemma 1. Parametrizing the complex function $f(s)$ for the circle ω_0, we obtain

$$g(\varphi) = f(s_k + \rho e^{i\varphi}) = 1/(\underbrace{1 - 2^{-2i\pi k/\log 2 - \rho(\cos\varphi + i\sin\varphi)}}_{:=u(\varphi)}). \tag{7}$$

Next,

$$\begin{aligned} |u(\varphi)| &= |1 - 2^{-\rho\cos\varphi}(\cos(\rho\log 2\sin\varphi) - i\sin(\rho\log 2\sin\varphi))| \\ &= (\underbrace{1 - 2^{1-\rho\cos\varphi}\cos(\rho\log 2\sin\varphi) + 2^{-2\rho\cos\varphi}}_{:=v(\varphi)})^{1/2}. \end{aligned} \tag{8}$$

The function $v(\varphi)$ is periodic with period 2π and symmetric with respect to $\varphi = \pi$ (indeed, $v(\pi - \varphi) = v(\pi + \varphi)$. Hence the statement of the lemma reduces to solving

$$\min_{0\leqslant\varphi\leqslant\pi} v(\varphi).$$

Differentiating $v(\varphi)$, we get for $0 < \varphi < \pi$

$$\begin{aligned} v'(\varphi) &= 2^{1-\rho\cos\varphi}\rho\log 2 \\ &\times \underbrace{(2^{-\rho\cos\varphi}\sin\varphi - \sin\varphi\cos(\rho\log 2\sin\varphi) + \cos\varphi\sin(\rho\log 2\sin\varphi))}_{:=w(\varphi)>0} > 0. \end{aligned}$$

49 Indeed, with $r = \rho\log 2$ and
1^0. $(r,\varphi) \in (0, r_0) \times (0, \pi/2)$, we have

$$\begin{aligned} w(\varphi) &= e^{-r\cos\varphi}\sin\varphi - \sin\varphi\cos(r\sin\varphi) + \cos\varphi\sin(r\sin\varphi) \\ &\geqslant \left(1 - r\cos\varphi + \frac{1}{2}(r\cos\varphi)^2 - \frac{1}{6}(r\cos\varphi)^3\right)\sin\varphi \\ &- \left(1 - \frac{1}{2}(r\sin\varphi)^2 + \frac{1}{24}(r\sin\varphi)^4\right)\underbrace{\sin\varphi}_{>0} + \left(r\sin\varphi - \frac{1}{6}(r\sin\varphi)^3\right)\underbrace{\cos\varphi}_{>0} \\ &= \frac{1}{24}r^2\sin\varphi\left(12 - 4r\cos\varphi - r^2\sin^4\varphi\right) > 0. \end{aligned}$$

2^0. For $(r,\varphi) \in (0, r_0) \times (\pi/2, \pi)$, we have

$$\begin{aligned} w(\varphi) &= e^{-r\cos\varphi}\sin\varphi - \sin\varphi\cos(r\sin\varphi) + \cos\varphi\sin(r\sin\varphi) \\ &\geqslant \left(1 - r\cos\varphi + \frac{1}{2}(r\cos\varphi)^2\right)\sin\varphi \\ &- \left(1 - \frac{1}{2}(r\sin\varphi)^2 + \frac{1}{24}(r\sin\varphi)^4\right)\underbrace{\sin\varphi}_{>0} + r\sin\varphi\underbrace{\cos\varphi}_{<0} \\ &= \frac{1}{24}r^2\sin\varphi\left(12 - r^2\sin^4\varphi\right) > 0. \end{aligned}$$

Preprints (www.preprints.org) | NOT PEER-REVIEWED | Posted: 10 May 2022 doi:10.20944/preprints202205.0122.v1

Note that $w(\pi/2) > 0$, thus the function $v(\varphi)$ is monotonically increasing and

$$v_{min} = \min_{0 \leqslant \varphi \leqslant \pi} v(\varphi) = v(0) = (1 - 2^{-\rho})^2,$$

with (7) and (8) yielding us the statement of the lemma. □

The error term and the computational complexity are closely linked to the problem of the selection of the minimal number of terms in the series (3). Let us formulate the following proposition.

Proposition 1. *Let $\sigma \geqslant 1/2$, $t \geqslant 0$, $\varepsilon > 0$ and $|s - s_k| \geqslant \varepsilon$, then*

(i) the error term of the series (3) is

$$|\gamma_n^{(j)}(s)| \leqslant G_n^{(j)} \frac{(\cosh \pi t)^{1/2}}{|1 - 2^{1-s}|}, \tag{9}$$

(ii) the series (3) to compute the Riemann zeta-function with d decimal digits of accuracy, require a number of terms

$$n^{(j)} = \left\lceil B_1^{(j)} t + B_2^{(j)} d + C_\varepsilon^{(j)} \right\rceil, \tag{10}$$

with coefficients of expressions (9) and (10) presented in Table 1.

Table 1. Coefficients of expressions (9) and (10).

j	$G_n^{(j)}$	$B_1^{(j)}$	$B_2^{(j)}$	$C_\varepsilon^{(j)}$
1	$\frac{2}{(3+\sqrt{8})^n}$	$\frac{\pi/2}{\log(3+\sqrt{8})}$	$\frac{\log 10}{\log(3+\sqrt{8})}$	$\frac{\log 2 - \log(1-2^{-\varepsilon})}{\log(3+\sqrt{8})}$
2	$\frac{1}{2^{n+1}}$	$\frac{\pi/2}{\log 2}$	$\frac{\log 10}{\log 2}$	$\frac{-\log 2 - \log(1-2^{-\varepsilon})}{\log 2}$

Proof of Proposition 1. Let us start with MB-series. The error term of the series (3) is (cf. Alg. 2 in [7])

$$|\gamma_n^{(1)}(s)| \leqslant \frac{2}{(3+\sqrt{8})^n} \frac{1}{|1 - 2^{1-s}|} \frac{1}{|\Gamma(s)|} \underbrace{\int_0^1 \frac{(-\log x)^{\sigma-1}}{1+x} dx}_{:= I(\sigma)}. \tag{11}$$

Considering the function $I(\sigma)$, we have

$$I(\sigma) \leqslant \int_0^1 (-\log x)^{\sigma-1} dx = \Gamma(\sigma). \tag{12}$$

By a product representation of the gamma function (cf. 8.326.1 in [10]),

$$\left| \frac{\Gamma(\sigma)}{\Gamma(s)} \right|^2 = \prod_{n=0}^{\infty} \left(1 + \frac{t^2}{(\sigma+n)^2} \right),$$

The product is decreasing by σ, hence (cf. 8.332.2 in [10]),

$$\frac{\Gamma(\sigma)}{|\Gamma(s)|} \leqslant \frac{\Gamma(\frac{1}{2})}{|\Gamma(\frac{1}{2} + it)|} = \frac{\sqrt{\pi}}{\sqrt{\frac{\pi}{\cosh \pi t}}} = \sqrt{\cosh \pi t}. \tag{13}$$

Preprints (www.preprints.org) | NOT PEER-REVIEWED | Posted: 10 May 2022 doi:10.20944/preprints202205.0122.v1

Hence,

$$|\gamma_n^{(1)}(s)| \leqslant \frac{2}{(3+\sqrt{8})^n} \frac{\sqrt{\cosh \pi t}}{|1-2^{1-s}|}. \tag{14}$$

In view of (14), to compute the Riemann zeta-function with d decimal digits of accuracy, the approach requires a number n of terms not less than

$$\begin{aligned} N_d(\sigma,t) &= \frac{\log 2 + d\log 10 + \frac{1}{2}\log\cosh \pi t - \log|1-2^{1-s}|}{\log(3+\sqrt{8})} \\ &= \frac{\pi t + \log(1+e^{-2\pi t}) + \log 2 + 2d\log 10 - 2\log|1-2^{1-s}|}{2\log(3+\sqrt{8})} \\ &\leqslant \frac{\pi t + 2d\log 10 - 2\log|1-2^{1-s}| + 2\log 2}{2\log(3+\sqrt{8})}. \end{aligned} \tag{15}$$

1^0. Let $|\sigma - 1| > \varepsilon$. We have

$$\begin{aligned} N_d(\sigma,t) &\leqslant \frac{\pi t + 2d\log 10 - 2\log|1-2^{1-\sigma}| + 2\log 2}{2\log(3+\sqrt{8})} \\ &\leqslant \frac{\pi/2}{\log(3+\sqrt{8})} t + \frac{\log 10}{\log(3+\sqrt{8})} d + \frac{\log 2 - \log(1-2^{-\varepsilon})}{\log(3+\sqrt{8})}. \end{aligned} \tag{16}$$

2^0. Let $|s - s_k| \geqslant \varepsilon$ and $|\sigma - 1| \leqslant \varepsilon$. By applying the maximum modulus principle and Lemma 1, we receive

$$\begin{aligned} N_d(\sigma,t) &\leqslant \frac{\pi t + 2d\log 10 - 2\log|1-2^{-\varepsilon}| + 2\log 2}{2\log(3+\sqrt{8})} \\ &= \underbrace{\frac{\pi/2}{\log(3+\sqrt{8})}}_{:=B_1^{(1)}} t + \underbrace{\frac{\log 10}{\log(3+\sqrt{8})}}_{:=B_2^{(1)}} d + \underbrace{\frac{\log 2 - \log(1-2^{-\varepsilon})}{\log(3+\sqrt{8})}}_{C_\varepsilon^{(1)}}, \end{aligned} \tag{17}$$

thus concluding the proof. The deduction for *BLC*-series is analogical. □

Corollary 1. *Under the conditions of Proposition 1, for $\varepsilon = 10^{-m}$, $m \in \mathbb{N}$, the series (3) to compute the Riemann zeta-function with d decimal digits of accuracy, requires the number of terms*

$$n^{(j)} = \left\lceil B_1^{(j)} t + B_2^{(j)}(d+m) \right\rceil + 2 - j. \tag{18}$$

Proof of Corollary 1. The result (18) follows immediately, if we notice that for $\varepsilon \to 0$ we have

$$\log(1-2^{-\varepsilon}) = \log\varepsilon + \log\log 2 + o(1).$$

□

NA-modifications of MB- and BLC-algorithms

Limit theorems for coefficients of *MB*- and *BLC*-series enable us to derive a normal approximation for coefficients $c_{n,k}^{(j)}$ (cf. (24) in [5]). We can formulate the following proposition.

Proposition 2. *Coefficients $c_{n,k}^{(j)}$ of the series (3) satisfy*

$$c_{n,k}^{(j)} = \overline{\Phi}\left(\frac{k-\mu_n^{(j)}}{\sigma_n^{(j)}}\right) + O\left(\frac{1}{\sqrt{n}}\right). \tag{19}$$

Preprints (www.preprints.org) | NOT PEER-REVIEWED | Posted: 10 May 2022 doi:10.20944/preprints202205.0122.v1

Coefficients $\mu_n^{(j)}$ and $\sigma_n^{(j)}$ are presented in Table 2.

Table 2. Coefficients of the expression (19).

j	$\mu_n^{(j)}$	$\sigma_n^{(j)}$
1	$\frac{n}{\sqrt{2}}$	$\frac{\sqrt{n}}{\sqrt[4]{32}}$
2	$\frac{n}{2}$	$\frac{\sqrt{n}}{2}$

Proof of Proposition 2. Let us start with MB-series coefficients. Suppose A_n is an integral random variable with the probability mass function

$$P(A_n = k) = \frac{u_{n,k}}{\sum_{j=0}^{n} u_{n,j}}, \quad k = 0, \dots, n. \tag{20}$$

Here (cf. (1) in [5])

$$u_{n,k} = n\frac{(n+k-1)!4^k}{(n-k)!(2k)!}, \quad n \in \mathbb{N}, \ \ 0 \leqslant k \leqslant n. \tag{21}$$

Thus,

$$c_{n,k}^{(1)} = 1 - \frac{\sum_{j=0}^{k} u_{n,j}}{\sum_{j=0}^{n} u_{n,j}}. \tag{22}$$

Let $F_n(x)$ be the cumulative distribution function of the random variable A_n (20), then (cf. Theorem 3 in [3])

$$F_n(\sigma_n^{(1)}x + \mu_n^{(1)}) = \Phi(x) + O\left(\frac{1}{\sqrt{n}}\right), \qquad x \in \mathbb{R}. \tag{23}$$

Note that the cumulative distribution function

$$F_n\left(\sigma_n^{(1)}x + \mu_n^{(1)}\right) = \sum_{j \leqslant \sigma_n^{(1)}x + \mu_n^{(1)}} \frac{u_{nj}}{\sum_{j=0}^{n} u_{nj}}.$$

Denoting $k = \lfloor \sigma_n x + \mu_n \rfloor$ and taking into account (22) and (23), we obtain

$$1 - c_{n,k}^{(1)} = \Phi\left(\frac{k - \mu_n^{(1)}}{\sigma_n^{(1)}}\right) + O\left(\frac{1}{\sqrt{n}}\right).$$

The first part of the proposition follows. Similar result for BLC-coefficients $c_{n,k}^{(2)}$ has been proven in [4]. □

Proposition 2 allows us to choose the number of terms $n^{(j)}$ for the series (3),

$$n^{(j)} = \lceil \mu_n^{(j)} + z_d \sigma_n^{(j)} \rceil, \tag{24}$$

for n large enough. Here $z_d = \Phi^{-1}(1 - 10^{-d})$. Note that

$$n^{(1)} \sim \underbrace{\frac{\pi}{2\sqrt{2}\log(3+\sqrt{8})}}_{=0.630\dots} t, \qquad n^{(2)} \sim \underbrace{\frac{\pi}{4\log 2}}_{=1.133\dots} t,$$

for fixed σ and d. The refined version of NA-modification based methodology is summarized in Algorithm 2 (see Section 4).

Preprints (www.preprints.org) | NOT PEER-REVIEWED | Posted: 10 May 2022 doi:10.20944/preprints202205.0122.v1

Empirical insights for NA-modifications

While performing practical computations using NA-algorithms, we have noticed that the values produced were significantly more accurate than otherwise implied by d in the analytic estimate (10). In order to increase the performance and to have a clear course for future theoretical refinements, we propose empirical formulae for the minimum number of terms in the series (3) to compute the Riemann zeta-function with d decimal digits of accuracy.

In [12] Kuzma proposed the following empirically-based estimate for the number of terms for the BLC-series ($d = 6$),

$$n^{(0)} = \lceil 0.67658827t + 113.26486067 \rceil. \tag{25}$$

In the present section we offer an improvement to this estimate.

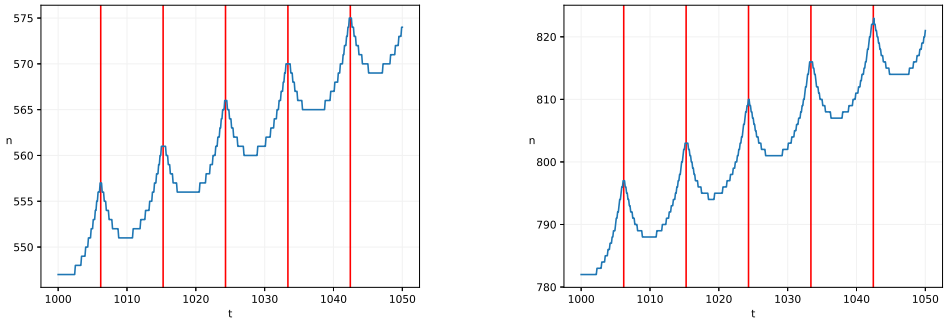

(a) NA-algorithm **(b)** BLC-algorithm

Figure 1. Periodic peaks of the minimum number of terms in series (3) for $d = 6$ digits of accuracy at $(\sigma, t) \in 1/2 \times [1000, 1050]$.

Figure 1 displays the minimum n required to calculate the Riemann zeta function with $d = 6$ digits of accuracy using NA- and BLC-algorithms at $\sigma = 1/2$, $t \in [1000, 1050]$ (the blue curve). The curves has clearly visible periodic peaks (marked by red vertical lines). The peaks have a period of $\lambda = 2\pi / \log 2$, which correspond s_k special points of Proposition 1. Since we are interested in the upper bound of this empirical curve, for the following calculations we use the points $t = \lambda k$, $k \in \mathbb{N}$.

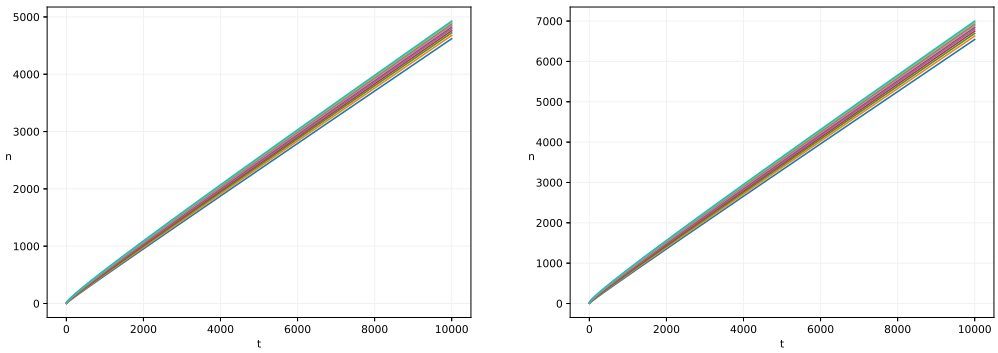

(a) NA-algorithm **(b)** BLC-algorithm

Figure 2. Regression models (26) for the minimum number of terms in series (3).

Figure 2 shows regression models

$$n^{(j)} = \left\lceil a^{(j)} t + b^{(j)} \sqrt{t} + c^{(j)} \right\rceil \tag{26}$$

Preprints (www.preprints.org) | NOT PEER-REVIEWED | Posted: 10 May 2022 doi:10.20944/preprints202205.0122.v1

derived for $d \in [1, 10]$ using the points $(\sigma, t) \in 1/2 \times (0, 10000)$. Each graph represents a fitted curve for a different d value.

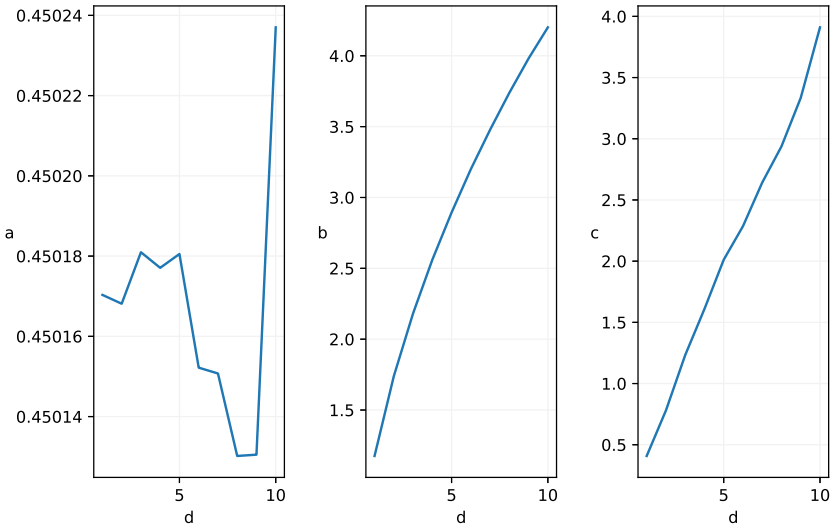

Figure 3. Coefficients of the regression models $a^{(1)}$, $b^{(1)}$ and $c^{(1)}$ plotted against the decimal digits of accuracy.

Figure 3 illustrates fluctuations of the coefficients of the regression models (26) by d. Here we can clearly see that $a^{(1)}$ has no correlation with d while $b^{(1)}$ and $c^{(1)}$ does.

Fitting $b^{(j)}$ with $b^{(j)} = x\sqrt{d} + y$ and $c^{(j)}$ with $c^{(1)} = xd + y$ we obtain the following coefficients for (26) (see Table 3):

Table 3. Coefficients of the regression model (26).

j	$a_n^{(j)}$	$b^{(j)}$	$c^{(j)}$
1	0.451	$1.407\sqrt{d} - 0.245$	$0.371d + 0.195$
2	0.637	$2.026\sqrt{d} - 0.272$	$1.602d - 0.026$

3. Visualizations of fractal structures associated with the Riemann zeta function

Methods of the visualization

In this study we employ two methods to reveal the Riemann zeta function underlying nature. The first heuristic method (FH-method) calculates RGB colors of the graph of the Riemann zeta function, using a composition of special functions. Suppose we have a function $f : (\mathbb{R}^+, \mathbb{C}) \to \mathbb{N}_0$:

$$f(x,z) = \begin{cases} \lfloor x \log |z| \rfloor, & \text{if} \quad z \neq 0, \\ 0, & \text{if} \quad z = 0. \end{cases} \tag{27}$$

Now we can define functions f_1, f_2, f_3:

$$f_1(x,z) = f(a, \zeta(s)), \qquad f_2(x,z) = f(b, \Re(\zeta(s))), \qquad f_3(x,z) = f(c, \Im(\zeta(s))). \tag{28}$$

Next, we calculate (R, G, B) colors of each pixel of the graph of the Riemann zeta function using polynomial functions of f_k (see Table 4):

$$\begin{aligned} R &= g_1^{(l)}(f_1, f_2, f_3) \mod 256, \\ G &= g_2^{(l)}(f_1, f_2, f_3) \mod 256, \\ B &= g_3^{(l)}(f_1, f_2, f_3) \mod 256. \end{aligned}$$

Preprints (www.preprints.org) | NOT PEER-REVIEWED | Posted: 10 May 2022 doi:10.20944/preprints202205.0122.v1

Table 4. List of $g_k^{(l)}$ functions.

l	$g_1^{(l)}$	$g_2^{(l)}$	$g_3^{(l)}$
1	f_1	f_2	f_3
2	$255 - f_1 f_2 f_3$	$f_2 f_3$	$255 - f_2$
2	f_1	f_2	f_3^2
4	$f_1 f_3$	f_2	f_3
5	$f_1 f_3$	$f_2 f_3$	f_3

The second approach (second fractal heuristic (SFH) method) is based on the application of the Mandelbrot set to the visualization of the Riemann zeta function. Suppose we aim to visualize $\zeta(\sigma + it)$ for $(\sigma, t) \in (\sigma_1, \sigma_2) \times (t_1, t_2)$. First, we introduce the log-transformation for each point (x, y) of the graph,

$$\begin{cases} x = L(\Re(\zeta(\sigma + it))), \\ y = L(\Im(\zeta(\sigma + it))), \end{cases} \tag{29}$$

thus obtaining the set $Q = (x_{min}, y_{min}) \times (x_{max}, y_{max})$. Here

$$L(x) = \begin{cases} \log|x|, & \text{if } x \neq 0, \\ 0, & \text{if } x = 0. \end{cases} \tag{30}$$

Next we linearly transform Q into the subset S of the complex plane,

$$(x, y) \in Q \to (x^*, y^*) \in S.$$

We take $S = (-2, 0.47) \times (-1.12i, 1.12i)$, where the Mandelbrot set is defined. Then we use an algorithm to generate the Mandelbrot set, setting the start position at $z_0 = 0$ and $z^* = (x^*, y^*)$:

$$z_{k+1} \leftarrow z_k^2 + z^*. \tag{31}$$

Suppose that $k \in \mathbb{N}$, $k \leqslant v_{max}$ indicates the number of iterations (31), required to ascertain that z^* does not belong to the Mandelbrot set, with

$$|z_{k+1}| \leqslant 2 \quad \text{and} \quad k < v_{max}.$$

For $k = v_{max}$, it is unclear if z^* does not belong to the Mandelbrot set. Now let $k_0 = \lfloor 50k \rfloor$. We calculate RGB color for the z^* point by the following rule:

$$RGB = \begin{cases} (0, & 0, & 0), & \text{if } k = v_{max}, \\ (255, & 255, & k_0 \mod 256), & \text{if } 510 < k_0 < v_{max}, \\ (100, & k_0 \mod 256, & 255), & \text{if } 255 < k_0 \leqslant 510, \\ (0, & 0, & k_0 \mod 256), & \text{if } k_0 \leqslant 255. \end{cases}$$

Visual investigations

The first visualization (see Figure 4) reveals the underlying structures in the "center" $S_1 \subset \mathbb{C}$ of the Riemann zeta function, received by two different methods (the color visualization and the fractal visualization). Here $S_1 = (-20, 8) \times (-14, 14)$. Figure 4a is obtained using FH-method with color parameters $a = 100$ and $b = c = 8$. The color transform $g_k^{(1)}$ is linear (see Table 4). Figure 4b is obtained using SFH-method. Note small bright fractal feature on the right-hand side, calling for in-depth investigation (see Figure 6).

Preprints (www.preprints.org) | NOT PEER-REVIEWED | Posted: 10 May 2022 doi:10.20944/preprints202205.0122.v1

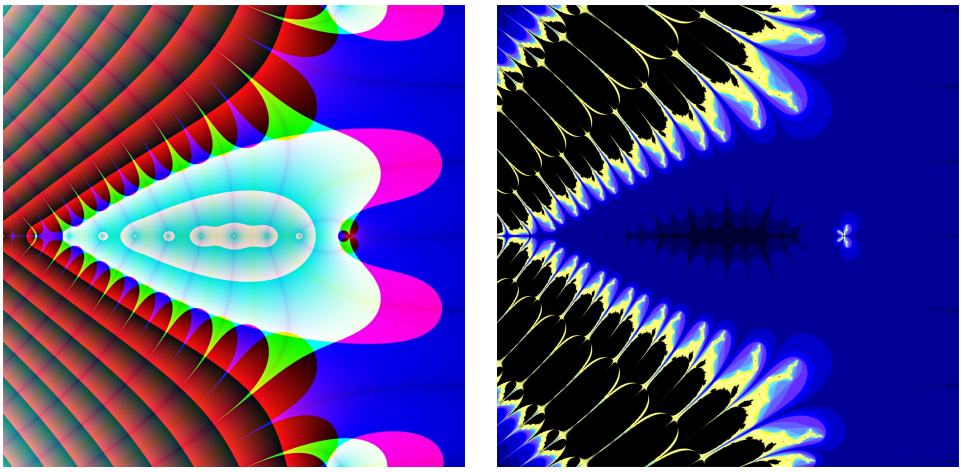

(a) Method 1: Color visualization **(b)** Method 2: Fractal visualization

Figure 4. The structures of the "center" of the Riemann zeta function, $(\sigma, t) \in (-20, 8) \times (-14, 14)$, received by SH and SFH methods. Note small fractal feature on the right-hand side of Fig. 4b.

Figure 5 presents zoom-in frames of S_2 region for the Riemann zeta function. Here $S_2 = (-5, 6) \times (\beta, \alpha + \beta)$, with four shifted in β intervals (see Table 5 for the ranges). The frames were received using FH-method with color parameters $a = 100$ and $b = c = 8$. The color transform $g_k^{(1)}$ is linear (see Table 4). Note nontrivial zeros of the Riemann zeta function (blue disks, marked with arrows in Fig. 4a and 4b).

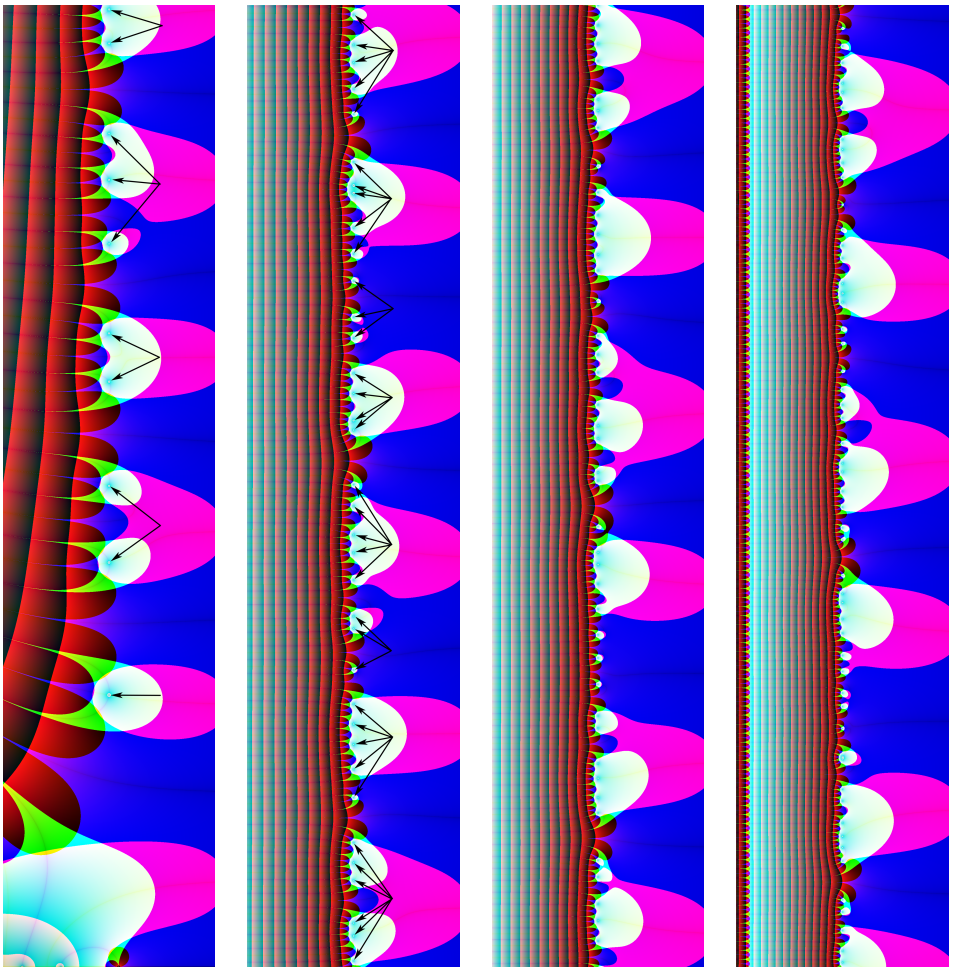

(a) **(b)** **(c)** **(d)**

Figure 5. FH-based zoomed-in frames of the Riemann zeta function (see Table 5 for the ranges).

Preprints (www.preprints.org) | NOT PEER-REVIEWED | Posted: 10 May 2022 doi:10.20944/preprints202205.0122.v1

Table 5. Ranges of the sets of Figure 5: $(\sigma, t) \in S_2$, $\alpha = 50$.

Figure	β	S_2
5a	0	$(-5, 6) \times (0, 50)$
5b	500	$(-5, 6) \times (500, 550)$
5c	1000	$(-5, 6) \times (1000, 1050)$
5d	5000	$(-5, 6) \times (5000, 5050)$

Figure 6 (obtained by SFH-method) extends the investigation of the fractal feature, associated with the Riemann zeta function, observed in Figure 4b. The frame 6a represents zoomed-in image of the feature in the range $(0.2, 2.2) \times (-1.6, 1.6)$. The frame 6b is the next magnification step, belonging to the range $(0.95, 1.05) \times (-0.08, 0.08)$. Fractal structures received in 6b are examined further in Figure 7.

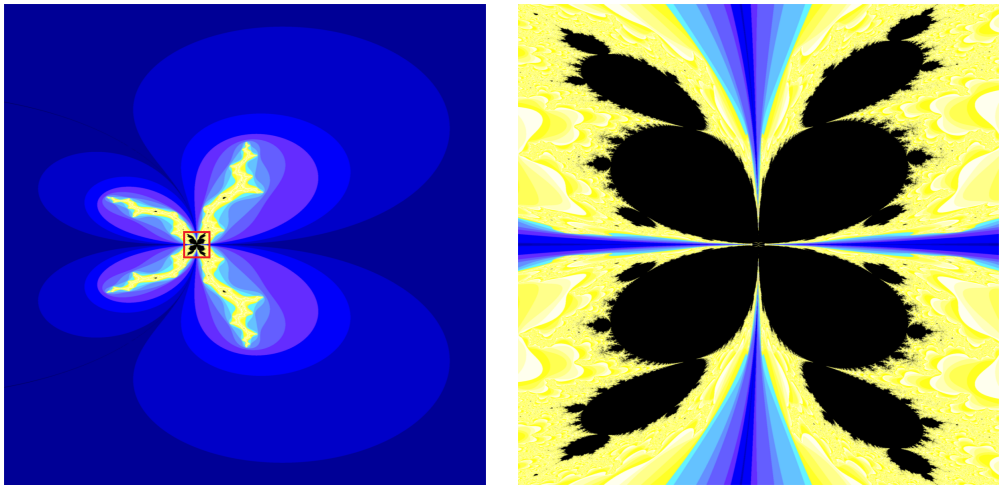

(a) **(b)**

Figure 6. Fractal features of the Riemann zeta function in the pole area (see Table 6 for the ranges).

Table 6. Ranges of the sets of Figure 6, $(\sigma, t) \in S_3$.

Figure	S_3
6a	$(0.20, 2.20) \times (-1.60, 1.60)$
6b	$(0.95, 1.05) \times (-0.08, 0.08)$

Figure 7a displays zoomed-in frame of the fractal border presented in Figure 6b. The next five frames (each of them corresponds to a colored rectangle in 7a) uncover some aesthetically pleasing features of fractal structures associated with the Riemann zeta function. Note snowflake-shaped fractals in Figure 7c, as well as pinwheel-shaped ones in Figure 7d and Figure 7e, resembling discs of spiral galaxies. Clockwise spinning 7e reminds us of the grand design spiral galaxy NGC 4254 in Coma Berenices. Counterclockwise rotating 7d resembles the Pinwheel Galaxy NGC 5457 in Ursa Major. Invariant features of fractal geometry generated from images provide a good set of descriptive values for the recognition of regions and objects, e.g., fractal signatures of galaxies are examined with the aim of classifying them (cf. [13]). Figure 7 is received by SFH-method. The ranges of the sets are given in Table 7.

Preprints (www.preprints.org) | NOT PEER-REVIEWED | Posted: 10 May 2022 doi:10.20944/preprints202205.0122.v1

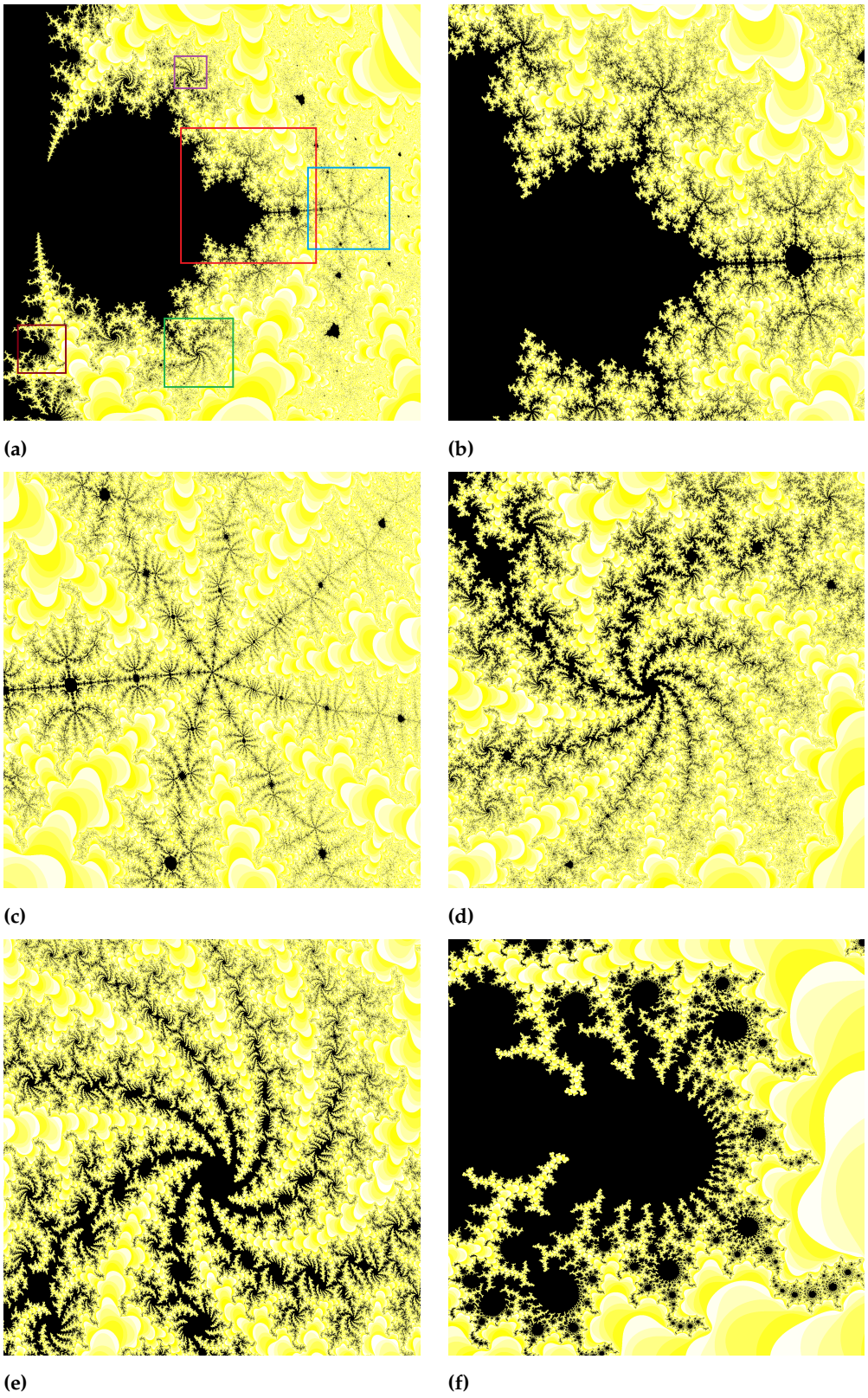

Figure 7. Fractal structures associated with the near-pole region of the Riemann zeta function. Frames 7b- 7f are zoomed-in rectangles of 7a. Ranges of the sets are given in Table 7.

Preprints (www.preprints.org) | NOT PEER-REVIEWED | Posted: 10 May 2022 doi:10.20944/preprints202205.0122.v1

Table 7. Ranges of the frames of Figure 6.

Figure	σ_1	σ_2	t_1	t_2
7a	1.30000	1.04000	-0.034000	-0.024000
7b	1.03730	1.03925	-0.029875	-0.027925
7c	1.03730	1.03925	-0.029875	-0.027925
7d	1.03385	1.03550	-0.033200	-0.031550
7e	1.03410	1.03485	-0.026000	-0.025250
7f	1.03035	1.03150	-0.032850	-0.031700

Figure 8 illustrates other facets of the geography of the Riemann zeta function. Graphs for the range $(-30, 10) \times (-14, 16)$ are obtained using four different non-linear color transformations $g_k^{(l)}$, where $g_1^{(l)} \neq f_1$ or $g_2^{(l)} \neq f_3$ or $g_3^{(l)} \neq f_3$. Color parameters are given in Table 8.

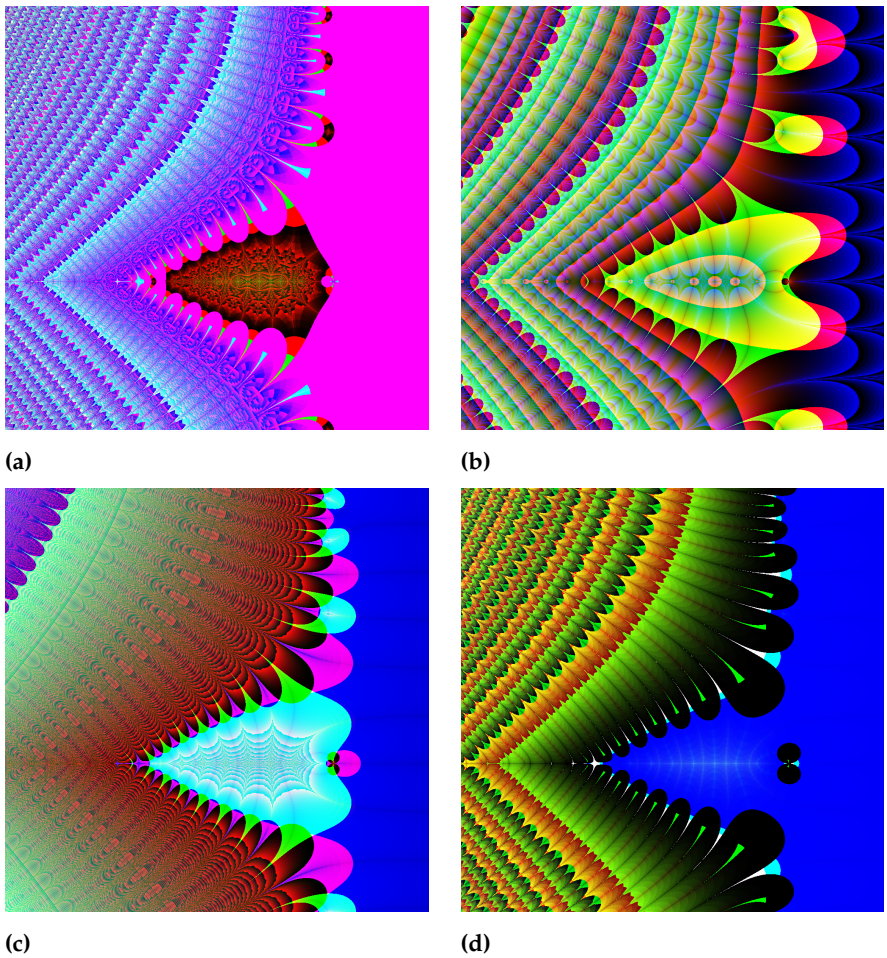

(a) **(b)** **(c)** **(d)**

Figure 8. Four non-linear color maps of the Riemann zeta function for $(\sigma, t) \in (-30, 10) \times (-14, 16)$. Color parameters are given in Table 8.

Table 8. Color parameters of Figure 8.

Figure	a	b	c	$g_k^{(l)}$
8a	10	1	2	$g_k^{(2)}$
8b	90	17	50	$g_k^{(3)}$
8c	9	7	5	$g_k^{(4)}$
8d	1	2	1	$g_k^{(5)}$

Preprints (www.preprints.org) | NOT PEER-REVIEWED | Posted: 10 May 2022 doi:10.20944/preprints202205.0122.v1

4. Computation and visualization algorithms

This section gives pseudocodes of the algorithms described in Sections 2 and 3.

Computation algorithms

The first algorithm outlines *MB*- and *BLC*-approaches (cf. Proposition 1 and Corollary 1) with the corresponding empirical modifications (26) for the calculation of multiple values of the Riemann zeta functions while t is fixed.

Algorithm 1 This algorithm will return multiple values of the Riemann zeta function for fixed t and array $\{\sigma_r\}$. Note that $L_k = \log k$ stand for precalculated logarithms.

procedure ZETA.M(σ : array [1..N] of real numbers; d, m, j : natural numbers; t : real number) ▷ (see Table 9)

$$n \leftarrow \begin{cases} \left\lceil ((\pi/2)t + (d+m)L_{10})/\log(3+\sqrt{8}) \right\rceil + 1, & j = 1, \\ \left\lceil ((\pi/2)t + (d+m)L_{10})/L_2 \right\rceil, & j = 2, \\ \left\lceil a^{(j-4)}t + b^{(j-4)}\sqrt{t} + c^{(j-4)} \right\rceil, & j = 5 \text{ or } j = 6 \end{cases}$$

  if j is odd **then** ▷ MB^1- and EMB^5-block
    $T_0 \leftarrow -L_n, \quad l_{max} \leftarrow \lfloor n/\sqrt{2} \rfloor$
    for $l \in \{1..n\}$ **do**
      $T_l \leftarrow T_{l-1} + L_{n-l+1} + L_{n+l-1} - L_{2l-1} - L_{2l}$
    end for
    $H_0 \leftarrow \exp(T_0 - T_{l_{max}} - l_{max}L_4)$
    for $l \in \{1..n\}$ **do**
      $H_l \leftarrow H_{l-1} + \exp(T_l - T_{l_{max}} + (l - l_{max})L_4)$
    end for
    for $k \in \{0..n\}$ **do**
      $\hat{c}_{n,k}^{(j)} \leftarrow (1 - H_k/H_n)(\cos(tL_{k+1}) - i\sin(tL_{k+1}))$
    end for
  else ▷ BLC^2- and $EBLC^6$ block
    for $k \in \{0..n\}$ **do**
      $\hat{c}_{n,k}^{(j)} \leftarrow (\cos(tL_{k+1}) - i\sin(tL_{k+1}))\text{betainc}(k+1, n-k+1, 0.5)$
    end for
  end if
  $\lambda \leftarrow 2(\cos(tL_2) - i\sin(tL_2))$
  for $r \in \{1..N\}$ **do** ▷ Calculation of *MB*- or *BLC*-series for the corresponding σ_r
    $S \leftarrow 0, \quad p \leftarrow -1$
    for $k \in \{0..n\}$ **do**
      $p \leftarrow -p$
      $S \leftarrow S + p\hat{c}_{n,k}^{(j)} \exp(-\sigma_r L_{k+1})$
    end for
    $S_r \leftarrow S/(1 - \lambda\exp(-\sigma_r L_2))$
  end for
return S ▷ Returns the array $S[1..N]$ of the Riemann zeta function values
end procedure

The second algorithm outlines *NA*-modifications of *MB*- and *BLC*-methods. These approaches are more suitable for the calculation of specific values of the Riemann zeta function.

Results of numerical experiments with Algorithm 1 and Algorithm 2 are presented in Section 5.

Preprints (www.preprints.org) | NOT PEER-REVIEWED | Posted: 10 May 2022 doi:10.20944/preprints202205.0122.v1

Algorithm 2 This algorithm will return values of the Riemann zeta function obtained by NA-modifications of MB- or BLC-method. Note that $L_k = \log k$ and $t > 10^3$.

function ZETA.NA(σ, t : real numbers; d, m, j : natural numbers)
  $n \leftarrow (\pi/2)t + (d+m)L_{10}$, $z \leftarrow \Phi^{-1}(1-10^{-d})$
  if $j = 1$ **then** ▷ $NAMB$-block
    $n \leftarrow (n + L_2 - \log L_2)/\log(3+\sqrt{8})$, $\mu_n \leftarrow n/\sqrt{2}$, $\sigma_n \leftarrow \sqrt{n}/\sqrt[4]{32}$
  else ▷ $NABLC$-block
    $n \leftarrow (n - L_2 - \log L_2)/L_2$, $\mu_n \leftarrow n/2$, $\sigma_n \leftarrow \sqrt{n}/2$
  end if
  $k_0 \leftarrow \lceil \mu_n + z\sigma_n \rceil$, $k_1 \leftarrow \mu_n - z\sigma_n$
  function C(n,k : nonnegative integers)
    if $k < k_1$ **then**
      $C \leftarrow 1$
    else
      $C \leftarrow 1 - \Phi((k-\mu_n)/\sigma_n)$
    end if
  end function
  $S \leftarrow 0$, $p \leftarrow -1$
  for $k \in \{0..k_0\}$ **do**
    $p \leftarrow -p$
    $S \leftarrow S + pC(n,k)\exp(-\sigma L_{k+1})(\cos(tL_{k+1}) - i\sin(tL_{k+1}))$
  end for
return $S/(1 - 2\exp(-\sigma L_2)(\cos(tL_2) - i\sin(tL_2)))$
end function

Visualization algorithms

The third algorithm, corresponding the first heuristic method (FH-method), calculates RGB colors of the graph of the Riemann zeta function, using a composition of special functions.

Algorithm 3 This algorithm will return a colored image of Riemann zeta function for $(\sigma, t) \in (\sigma_{\min}, \sigma_{\max}) \times (t_{\min}, t_{\max})$. Other parameters: a, b, c - color parameters, g_1, g_2, g_3 - polynomial functions of f_1, f_2, f_3 (see Table 4), w - width in pixels of output image img.

procedure FH($\sigma_{\min}$, $\sigma_{\max}$, $t_{\min}$, $t_{\max}$, a, b, c : real numbers; w : natural number)
  $h \leftarrow \lfloor w \cdot (t_{\max} - t_{\min})/(\sigma_{\max} - \sigma_{\min}) \rfloor$
  $img \leftarrow [\,]$
  for $j \in \{0..h-1\}$ **do**
    $row \leftarrow [\,]$
    $t \leftarrow t_{\min} + j \cdot (t_{\max} - t_{\min})/(h-1)$
    for $k \in \{0..w-1\}$ **do**
      $\sigma \leftarrow \sigma_{\min} + k \cdot (\sigma_{\max} - \sigma_{\min})/(w-1)$
      $z \leftarrow \zeta(\sigma + it)$
      $f_1 \leftarrow \lfloor a \log |z| \rfloor$
      $f_2 \leftarrow \lfloor b \log |\Re(z)| \rfloor$
      $f_3 \leftarrow \lfloor c \log |\Im(z)| \rfloor$
      $g_1 \leftarrow g_1(f_1, f_2, f_3)$
      $g_2 \leftarrow g_2(f_1, f_2, f_3)$
      $g_3 \leftarrow g_3(f_1, f_2, f_3)$
      $RGB \leftarrow [g_1 \mod 256, g_2 \mod 256, g_3 \mod 256]$
      $row \leftarrow row + RGB$
    end for
    $img \leftarrow img + row$
  end for
end procedure

Preprints (www.preprints.org) | NOT PEER-REVIEWED | Posted: 10 May 2022 doi:10.20944/preprints202205.0122.v1

The fourth algorithm, corresponding the second fractal heuristic method (*SFH*-method), employs the Mandelbrot set to visualize the Riemann zeta function.

Algorithm 4 This algorithm will return fractalized image of Riemann zeta function for $(\sigma, t) \in (\sigma_{\min}, \sigma_{\max}) \times (t_{\min}, t_{\max})$. Here m stands for max iterations to get more precise fractal image, w - width in pixels of output image img. The output image utilizes yellow-black-blue color palette.

procedure SFH($\sigma_{\min}$, $\sigma_{\max}$, $t_{\min}$, $t_{\max}$: real numbers; w, m : natural numbers)
  $h \leftarrow \lfloor w \cdot (t_{\max} - t_{\min}) / (\sigma_{\max} - \sigma_{\min}) \rfloor$
  $img \leftarrow [\,]$
  $w_1 \leftarrow 2.47 / (\sigma_{\max} - \sigma_{\min})$
  $w_2 \leftarrow (0.47\sigma_{\min} + 2\sigma_{\max}) / (\sigma_{\min} - \sigma_{\max})$
  $w_3 \leftarrow 2.24 / (t_{\max} - t_{\min})$
  $w_4 \leftarrow 1.12(t_{\min} + t_{\max}) / (t_{\min} - t_{\max})$
  for $j \in \{0..h-1\}$ **do**
    $row \leftarrow [\,]$
    $t \leftarrow t_{\min} + j \cdot (t_{\max} - t_{\min}) / (h-1)$
    for $k \in \{0..w-1\}$ **do**
      $\sigma \leftarrow \sigma_{\min} + k \cdot (\sigma_{\max} - \sigma_{\min}) / (w-1)$
      $z \leftarrow \zeta(\sigma + it)$
      $z^* \leftarrow w_1 \text{sign}(\Re(z)) \log|\Re(z)| + w_2 + (w_3 \text{sign}(\Im(z)) \log|\Im(z)| + w_4)i$
      $z \leftarrow 0$
      $n \leftarrow 0$
      while $|z| \leqslant 2$ **and** $n < m$ **do**
        $z \leftarrow z^2 + z^*$
        $n \leftarrow n + 1$
      end while
      $RGB \leftarrow [0,\ 0,\ 0]$
      if $|z| > 2$ **then**
        $l \leftarrow \lfloor 50n \rfloor$
        if $l > 510$ **then**
          $RGB \leftarrow [255,\ 255,\ l \mod 256]$
        else if $l > 255$ **then**
          $RGB \leftarrow [100,\ l \mod 256,\ 255]$
        else
          $RGB \leftarrow [0,\ 0,\ l \mod 256]$
        end if
      end if
      $row \leftarrow row + RGB$
    end for
    $img \leftarrow img + row$
  end for
end procedure

5. Numerical experiments

We have performed numerical experiments with seven methods and modifications listed in Table 9.

Preprints (www.preprints.org) | NOT PEER-REVIEWED | Posted: 10 May 2022 doi:10.20944/preprints202205.0122.v1

Table 9. List of algorithms under examination.

j	Abbreviation	Algorithm
1	*MB*	modification of Borwein's efficient algorithm
2	*BLC*	series with binomial-like coefficients algorithm
3	*NAMB*	normal approximation-based modification of *MB*-algorithm
4	*NABLC*	normal approximation-based modification of *BLC*-algorithm
5	*EMB*	empirical modification of *MB*-algorithm
6	*EBLC*	empirical modification of *BLC*-algorithm
7	*ZF*	*Zetafast* algorithm

First numerical experiment

The first numerical experiment deals with normal approximation-based modifications (cf. Algorithm 2). Using *NAMB* ($j = 3$), *NABLC* ($j = 4$) and *Zetafast* ($j = 7$) methods we generate sequences of values of the Riemann zeta function $\{\zeta_{l,p}^{(j)}\}$, $1 \leqslant l \leqslant N$, $N = 10^5$, taking as arguments uniformly distributed $s_{l,p} \in S_p^{(1)}$. Here

$$S_p^{(1)} = \underbrace{(0.5, 1.5)}_{\sigma} \times \underbrace{(s_{k_p} + \rho_1, s_{k_{(p+1)}} - \rho_1)}_{t}, \tag{32}$$

where s_{k_p} stand for critical points (5) with $k_p = 2^{p+6}$, $1 \leqslant p \leqslant 3$, and $\rho_1 = 10^{-1}$. Thus we obtain 9 sequences overall (3 algorithms $\times$ 3 sets of arguments). Using *Zetafast* algorithm as a benchmark we calculate the accuracy $\delta_p^{(j)}$ and the relative performance $\theta_p^{(j)}$,

$$\delta_p^{(j)} = \max_{1 \leqslant l \leqslant N} \left| \zeta_{l,p}^{(j)} - \zeta_{l,p}^{(7)} \right|, \qquad \theta_p^{(j)} = \tau_p^{(j)} / \tau_p^{(7)}, \qquad 3 \leqslant j \leqslant 4, \tag{33}$$

where $\tau_p^{(j)}$ is the processing time of jth sequence $\{\zeta_{l,p}^{(j)}\}$, $1 \leqslant l \leqslant N$, for fixed p. The results of the first numerical experiment are presented in Table 10.

Table 10. Results of the first numerical experiment: accuracy $\delta_p^{(j)}$ and relative performance $\theta_p^{(j)}$, for $d = 6$, $m = 1$. The last line of the table shows the performance of *ZF*-algorithm (sec).

Method	j	$S_1^{(1)}$	$S_2^{(1)}$	$S_3^{(1)}$
NAMB	3	$1.80 \cdot 10^{-11}$ / 0.088	$1.60 \cdot 10^{-11}$ / 0.12	$2.90 \cdot 10^{-11}$ / 0.18
NABLC	4	$1.82 \cdot 10^{-11}$ / 0.22	$1.74 \cdot 10^{-11}$ / 0.32	$3.35 \cdot 10^{-11}$ / 0.45
ZF	7	86.72	121.04	172.95

Second numerical experiment

The second numerical experiment aims to verify the accuracy of the algorithms on fixed horizontal lines, close to critical points. Using *MB* ($j = 1$) and *BLC* ($j = 2$) methods, their empirical modifications ($j = 5$ and $j = 6$) and *Zetafast* method ($j = 7$), we generate (cf. Algorithm 1) sequences of values of the Riemann zeta function $\{\zeta_{l,p}^{(j)}\}$, $1 \leqslant l \leqslant N$, $N = 10^5$, taking as arguments uniformly distributed $s_{l,p} \in S_p^{(2)}$. Here

$$S_p^{(2)} = \underbrace{(0.5, 1.5)}_{\sigma} \times t_p, \qquad t_p = s_{k_p} + \rho_1, \qquad k_p = 2^{p+6}, \qquad 1 \leqslant p \leqslant 3. \tag{34}$$

Thus we obtain 15 sequences overall (5 algorithms $\times$ 3 sets of arguments). Using *Zetafast* algorithm as a benchmark we calculate the accuracy $\delta_p^{(j)}$ and the relative performance $\theta_p^{(j)}$ (cf. (33)). The results of the second numerical experiment are presented in Table 11.

Preprints (www.preprints.org) | NOT PEER-REVIEWED | Posted: 10 May 2022 doi:10.20944/preprints202205.0122.v1

Table 11. Results of the second numerical experiment: accuracy $\delta_p^{(j)}$ and relative performance $\theta_p^{(j)}$ on fixed lines t_p, for $d = 6$, $m = 1$. The last line shows the performance of ZF-algorithm (sec).

Method	j	$S_1^{(2)}$	$S_2^{(2)}$	$S_3^{(2)}$
MB	1	$1.68 \cdot 10^{-11}$	$1.46 \cdot 10^{-11}$	$2.65 \cdot 10^{-11}$
		0.04	0.055	0.078
BLC	2	$1.77 \cdot 10^{-11}$	$1.55 \cdot 10^{-11}$	$2.64 \cdot 10^{-11}$
		0.1	0.15	0.2
EMB	5	$6.43 \cdot 10^{-7}$	$5.62 \cdot 10^{-7}$	$5.51 \cdot 10^{-7}$
		0.024	0.032	0.044
$EBLC$	6	$7.07 \cdot 10^{-7}$	$7.78 \cdot 10^{-7}$	$7.84 \cdot 10^{-7}$
		0.034	0.048	0.065
ZF	7	86.64	121.29	173.14

The numerical experiments have been performed on Intel® Core™ i7-8750H 2.2GHz (boosted to 4.0 GHz) processor with 16GB DDR4 RAM. The code has been compiled with g++ 11.2.0 compiler using O3 optimization. C++ Boost library has been used for the implementation of the incomplete beta function for BLC-algorithm.

6. Discussion and concluding remarks

Discussion of the results

We have refined the error terms and the expressions for the minimal number of terms in MB- and BLC-series of efficient algorithms for the computation of the Riemann zeta function, taking into account the behavior of the series in the neighborhoods of critical points. Proposition 1 shows that MB-based algorithms converge faster than BLC-based algorithms. Indeed, MB-coefficient of the error term $G_n^{(1)} = O(0.172^n)$ while $G_n^{(2)} = O(0.5^n)$ (cf. (9)). However, BLC-approach has its advantages that might be useful in analytical research (cf. (4)). Note that this deficiency of MB-algorithm is solved by the introduction of NA-modification (19).

The results of the numerical experiments (see Table 10 and Table 11) show that MB and BLC methods, along with their normal and empirical modifications, allow fast and accurate calculations of the Riemann zeta function for large values of argument t. The results demonstrate that the introduced modifications accelerate computations of the Riemann zeta function, compared to *Zetafast* method. These versions of algorithms are well-suited for distributed computations and grid computing.

Findings of visual investigations of fractal structures, associated with the Riemann zeta function

The illustrations obtained using FH-method clearly show the arrangement of trivial and non-trivial zeros of the Riemann zeta function in the complex plane (see Figures 5a, 5b). In addition to these points, we can also see dark 2D curves that satisfy the conditions $\Re(\zeta(\sigma + it)) = 0$ and $\Im(\zeta(\sigma + it)) = 0$ (see Figure 4a). The SFH-method distributes deformed copies of the Mandelbrot set in the complex plane, thus relating the values of the Riemann zeta function to the fractal structure. This allows for a visual assessment of essential changes in the Riemann zeta function values. Next, SFH-approach reveals notable symmetric fractals characterizing the neighborhood of the pole of the Riemann zeta function (see Figure 6 and Figure 7).

Future research directions

Numerical experiments with empirical formulas indicate that the theoretical selection of the number of terms of the series n can be reduced. Next, the accuracy of the normal approximation-based modifications of MB and BLC algorithms might be refined by employing the theory of large deviations. The figures presented in this work reveal areas of the complex plane where the modulus of the Riemann zeta function exhibits very volatile values. This allows us to investigate the complex plane regions of

$\Re\zeta(s) = \Im\zeta(s)$, thus enabling us to locate non-trivial zeros' positions visually. In future works, these visual instruments could be refined.

Author Contributions: Conceptualization, I.B., M.S. and L.K.; methodology, I.B. and M.S.; software, M.S. and L.K.; validation, I.B., M.S. and L.K.; formal analysis, I.B.; investigation, I.B., M.S. and L.K.; resources, M.S. and L.K..; writing—original draft preparation, I.B., M.S. and L.K.; writing—review and editing, I.B.; visualization, M.S. and L.K.; supervision, I.B. All authors have read and agreed to the published version of the manuscript.

Funding: This research received no external funding.

Institutional Review Board Statement: Not applicable.

Informed Consent Statement: Not applicable.

Data Availability Statement: Not applicable.

Conflicts of Interest: The authors declare no conflict of interest.

Abbreviations

Abbreviations

The following abbreviations are used in this manuscript:

MB	Modification of Borwein's algorithm
BLC	Binomial-like coefficients
NA	Normal approximation
FH	First heuristic
SFH	Second fractal heuristic
NGC	New General Catalogue of Nebulae and Clusters of Stars

References

1. Belovas, I. A central limit theorem for coefficients of the modified Borwein method for the calculation of the Riemann zeta-function. *Lith. Math. J.* **2019**, *59(1)* , 17–23. DOI: 10.15388/LMR.B.2019.15208
2. Belovas, I. A local limit theorem for coefficients of modified Borwein's method. *Glas. Mat.* **2019**, *54(1)*, 1–9. DOI: 10.3336/gm.54.1.01
3. Belovas, I. Series with binomial-like coefficients for the Riemann zeta function, *Ann. Mat. Pura Appl.* **2022**, *201*, 903–912. DOI: 10.1007/s10231-021-01142-1
4. Belovas, I.; Sabaliauskas, M. Series with binomial-like coefficients for the evaluation and 3D visualization of zeta functions. *Informatica* **2020**, *31(4)*, 659–680. DOI: 10.15388/20-INFOR434
5. Belovas, I.; Sakalauskas, L.; Starikovičius, V. A method for accelerated computation of the Riemann zeta function on the complex plane. *Publ. Math. Debrecen* **2022** (in print) DOI: 10.5486/PMD.2022.9120
6. Blankers, V.; Rendfrey, T.; Shukert, A.; Shipman, P.D. Julia and Mandelbrot sets for dynamics over the hyperbolic numbers. *Fractal Fract.* **2019**, *3(1:6)*. DOI: 10.3390/fractalfract3010006
7. Borwein, P. An efficient algorithm for the Riemann zeta function. In *Constructive, Experimental, and Nonlinear Analysis (Limoges, 1999)* Canadian Mathematical Society Conference Proceedings **2000**, *27*, 29–34.
   URL: www.cecm.sfu.ca/personal/pborwein/PAPERS/P155.pdf
8. Coffey, M.W. An efficient algorithm for the Hurwitz zeta and related functions, *J. Comput. Appl. Math.* **2009**, *225(2)*, 338-346. DOI: 10.1016/j.cam.2008.07.040
9. Fischer, K. *The Zetafast algorithm for computing zeta functions* **2017**. arXiv:1703.01414
10. Gradshteyn, I. S.; Ryzhik, I. M. *Table of Integrals, Series, and Products*, 8th ed.; Academic Press, **2014**.
11. King, C. Fractal geography of the Riemann zeta function: Part I *Prespacetime Journal* **2012**, *3(4)*, 319–340.
    https://prespacetime.com/index.php/pst/article/view/357/352
12. Kuzma, L. Visualization of surfaces and 3D curves, associated with the Riemann zeta function and its non-trivial zeros arrangement (Bachelor thesis) **2021** URL: www.lvb.lt/permalink/f/16nmo04/ELABAETD107115273 (in Lithuanian)
13. Lekshmi, S.; Revathy, K.;,Prabhakaran Nayar, S.R. Galaxy classification using fractal signature, *Astron. Astrophys.* **2003**, *405(3)*, 1163–1167. DOI: 10.1051/0004-6361:20030541
14. Šleževičienė, R. An efficient algorithm for computing Dirichlet *L*-functions, *Integr. transf. spec. f.* **2004**, *15(6)*, 513-522, DOI: 10.1080/1065246042000272072
15. Tingen, L.L. The Julia and Mandelbrot sets for the Hurwitz zeta function (Master thesis) **2009**.
    http://dl.uncw.edu/Etd/2009-3/tingenl/larrytingen.pdf

 doi:10.20944/preprints202205.0122.v1

16. Vepštas, L. An efficient algorithm for accelerating the convergence of oscillatory series, useful for computing the polylogarithm and Hurwitz zeta functions. *Numer. Algorithms* **2008**, *47(3)*, 211–252. DOI: 10.1007/s11075-007-9153-8
17. Woon, S.C. Fractals of the Julia and Mandelbrot sets of the Riemann zeta function. https://arxiv.org/abs/chao-dyn/9812031